

# High Reynolds number effects in wall turbulence

Ivan Marusic, Romain Mathis, Nicholas Hutchins

Department of Mechanical Engineering, University of Melbourne, Victoria 3010, Australia

---

## Abstract

A review of recent advances in the study of high Reynolds number turbulent boundary layers is given. The emergent regime of very large-scale structures in the logarithmic region and their subsequent influence on the near-wall cycle challenges many of the previously held assumptions regarding scaling of turbulent boundary layers at high Reynolds numbers. Experimental results are presented to illustrate the superimposition of large-scale energy onto the near-wall cycle, together with an interaction well described by an amplitude modulation effect. Both phenomena are shown to increase in magnitude (as compared to viscous-scaled events) as Reynolds number increases. These observations lead to a possible model for a statistically representative near-wall velocity signal (giving accurate energy spectra) based on a given filtered velocity signal from the log region of a high Reynolds number turbulent flow.

*Key words:* Wall turbulence, Turbulent boundary layers, Reynolds number effects

---

## 1. Introduction

Wall-bounded turbulent flows have attracted considerable attention over many years, which is not surprising given their prevalence and importance in many engineering and scientific applications. Up until fairly recently a majority of studies have focused on the near-wall region of wall-bounded flows, and due to practical considerations, many of these investigations have also been conducted at low Reynolds numbers. To a large extent, such studies have their origins in the observations of near-wall streaks [25] in the velocity field and the realisation that recurrent near-wall structures can play a key role in turbulence regeneration. More recently our understanding of such events has tended to shift towards a self-sustaining near-wall cycle, in which the near-wall structures propagate and sustain without need of external triggers. Such autonomous views are based largely on insightful low Reynolds number simulations by Jimenez & Pinelli [22] and Schoppa & Hussain [49]. At low Reynolds numbers, the over-riding focus on the near-wall region is justified by the fact that the dominant kinetic energy production occurs within the viscous buffer layer, at a nominal wall-normal distance of  $z^+ = zU_\tau/\nu \approx 12$ .<sup>1</sup> This is demonstrated in figure 1(a), where an estimate for the turbulent kinetic energy production, defined as the product of Reynolds shear stress and mean shear

$$P = -\overline{uw}^+ \frac{dU^+}{dz^+}, \quad (1)$$

---

<sup>1</sup>Throughout this paper the coordinate system,  $x$ ,  $y$  and  $z$ , refers to the streamwise, spanwise and wall-normal directions, and the respective fluctuating velocity components are denoted by  $u$ ,  $v$  and  $w$ .  $U_\tau$  is friction velocity and  $\nu$  is the kinematic viscosity of the fluid, and the superscript + denotes normalization with viscous units.

is plotted for three Reynolds numbers,  $Re_\tau = 1000, 2000, 10^6$ . Here,  $Re_\tau = \delta U_\tau/\nu$ , where  $\delta$  is the boundary layer thickness. This plot is similar to that shown by Panton [42] in which a very small variation in the production curves was noted from low to high Reynolds numbers. Based on these observations, and the fact that the measurements of the mean velocity and the Reynolds shear stress showed the expected theoretical Reynolds number trends, Panton [42] commented: ‘*one could infer that physical processes producing  $\overline{uw}$  discovered at low Reynolds numbers are likely to also be relevant at higher values. This is not to say there will not be modifications or new events, however, it is likely that the dominant processes are roughly similar.*’ This sentiment has been a persistent narrative throughout the majority of literature pertaining to low Reynolds number flows. However, it should also be noted that production curves, when plotted semi-logarithmically as they are in figure 1(a), can be misleading. On these axes, if one considers the contribution to the global or bulk kinetic energy production (the contribution to the integral of  $P$ ), then the importance of the log region is not immediately clear, particularly as one goes from low to very high Reynolds numbers. The inset of figure 1(a) highlights the increasing production contribution due to the log region as Reynolds number increases. For a graphical representation, where equal areas indicate equal integral contributions, a premultiplied plot is required when using semi-logarithmic axes. This is shown in figure 1(b) and here it is clear that the contribution to the bulk production comes from the logarithmic region for sufficiently high Reynolds number. This is further illustrated in figure 2 where the contribution to the bulk or total production is compared for given regions in the boundary layer. The figure shows that the viscous near-wall region contribution to the bulk production is dominant at low Reynolds numbers but it is the log region that is the major contributor at high Reynolds numbers. The cross-over at which the contribution from the log

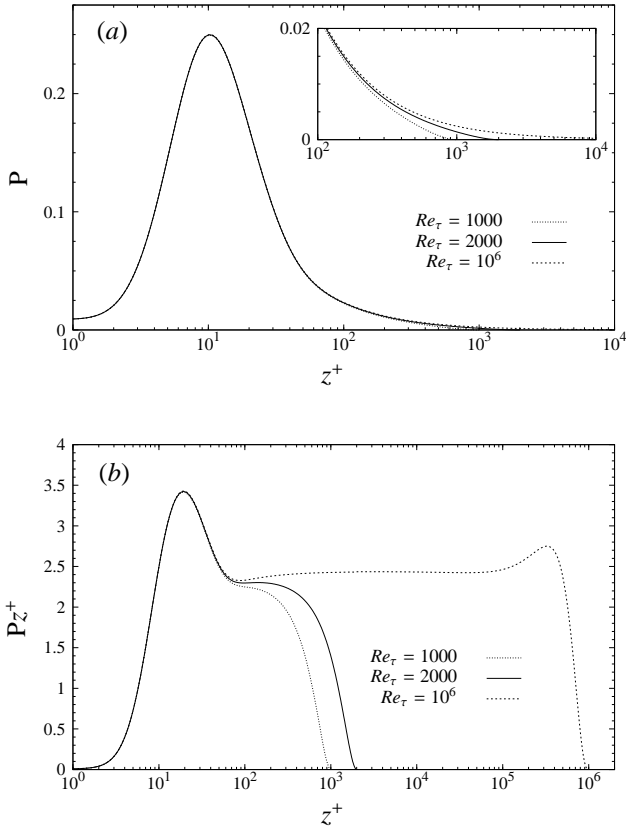


Figure 1: Turbulence kinetic energy production for a range of Reynolds numbers. Here  $P$  is estimated using the law of wall-wake formulation for mean velocity for ZPG boundary layers, and the corresponding Reynolds shear stress profile as given in Ref. [46]; (a) semi-logarithmic representation; (b) pre-multiplied version of figure 1(a).

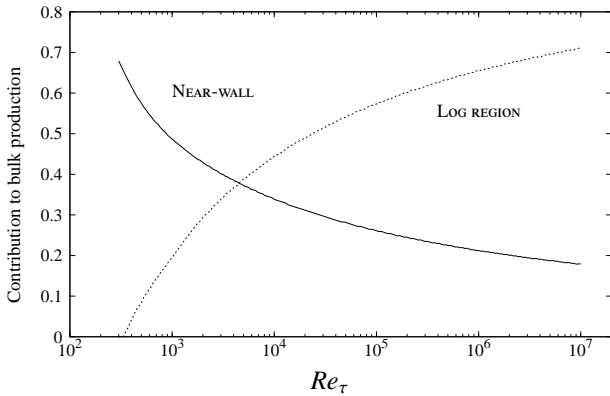


Figure 2: Ratio of contribution to kinetic energy production to bulk production. NEAR-WALL (solid line) refers to the viscous near-wall region contribution, taken as  $0 < z^+ < 30$ ; LOG REGION (dotted line) refers to contribution from the logarithmic region, taken nominally as  $70 < z^+ < 0.15Re_\tau$ .

region (taken tentatively to be  $70 < z^+ < 0.15Re_\tau$ ) is equal that from the near-wall region (taken tentatively to be  $0 < z^+ < 30$ ) is seen to be  $Re_\tau \approx 4200$ .

The question of how wall turbulence changes at high Reynolds numbers has received heightened interest over the last decade or so. This has resulted in the construction or planning of high Reynolds number facilities, including the Princeton *Superpipe* [52], the development of *SLTEST*, an atmospheric test facility in the Great Salt Lake Desert, Utah [24], and a series of high Reynolds number wind tunnel facilities in Chicago (NDF [39]), Stockholm (MTL [41]), Melbourne [40], Lille [5], and Stanford [7].

With these new measurements have come questions about measurement techniques [44, 18] in high Reynolds number regimes, and a re-examination of the boundary-layer scaling at high Reynolds number and its asymptotic scaling in the limit of infinite Reynolds number. Besides refinements of the ‘classic’ scaling (see e.g. Ref. [35]), new theories have been proposed questioning the form and basis of classic scaling laws [4, 11]. For existing data, the log-law appears to persist as the preferred description of the mean velocity profile in wall turbulence. However, open questions remain regarding the universality of its parameters, and the extent of the logarithmic overlap region. These issues are discussed further by Marusic *et al.* [30].

In this paper we will concentrate on issues related to the universality of the near-wall region and the influence of outer-flow motions on this near-wall region.

## 2. Experimental details

To consider the effect of increasing Reynolds number, experimental data measured by the authors are used. The data-sets come from boundary layer studies in three separate facilities, and a summary of the experimental parameters is given in Table 1. The lowest Reynolds number of  $Re_\tau = 500$  are hot-wire measurements in the boundary layer wind tunnel at the University of Nottingham, with full details of the experiments given by Hutchins [14]. The remaining laboratory data, over the range  $Re_\tau = 2800 - 19000$ , are from hot-wire measurements in the large boundary layer wind tunnel at the University of Melbourne (also known as HRNBLWT), which has a 27 m long working section. The full details of these experiments are given in a recent paper by Hutchins *et al.* [18]. The largest Reynolds number data are obtained from atmospheric surface layer using a wall-normal array of 9 sonic anemometers at SLTEST. Full details of the SLTEST conditions and set-up are given in Refs. [28, 15].

The measurements in the Melbourne tunnel were carried out with hot-wires that had sensing lengths matched to the same dimensionless length,  $l^+ = 22$ . This was done to avoid the complication of spatial resolution problems that are prevalent with many turbulence measurements in the near-wall region [18]. For this  $l^+$  value only a small amount of attenuation of the turbulent kinetic energy is expected. The Nottingham wind tunnel results were taken with a hot-wire with sensing length of  $l^+ = 8$ , and figure 3(a) shows the streamwise turbulence intensity profile across the boundary layer. Also, shown on the figure is the estimated value of turbulence intensity that a hot-wire with  $l^+ = 22$  would measure at  $z^+ = 15$ , the nominal position of the

$Re_\tau$	Facility	$\delta$ (m)	$U_\tau$ (m/s)	$U_\infty$ (m/s)	$l^+$	$\Delta T^+$	no. points	domain of measurement
500	Nottingham	0.071	0.114	2.46	8	0.9	43	$z^+ = 4.8 - z/\delta = 1.6$
2800	Melbourne	0.098	0.442	11.97	22	0.53	53	$z^+ = 9.1 - z/\delta = 2.0$
3900	Melbourne	0.140	0.426	11.87	22	0.49	49	$z^+ = 11.8 - z/\delta = 2.0$
7300	Melbourne	0.326	0.330	9.82	22	0.37	51	$z^+ = 5.5 - z/\delta = 1.4$
13600	Melbourne	0.315	0.671	20.63	22	0.48	54	$z^+ = 7.4 - z/\delta = 1.4$
19000	Melbourne	0.303	0.960	30.20	22	0.59	53	$z^+ = 8.7 - z/\delta = 1.4$
650000	SLTEST	60	0.180	–	850	96	9	$z/\delta = 0.02 - z/\delta = 0.43$

Table 1: Experimental parameters for turbulence measurements; Melbourne and Nottingham wind tunnel experiments were conducted with single hot-wire probe; SLTEST data were acquired with sonic anemometers. No. of points indicates the number of wall-normal positions.

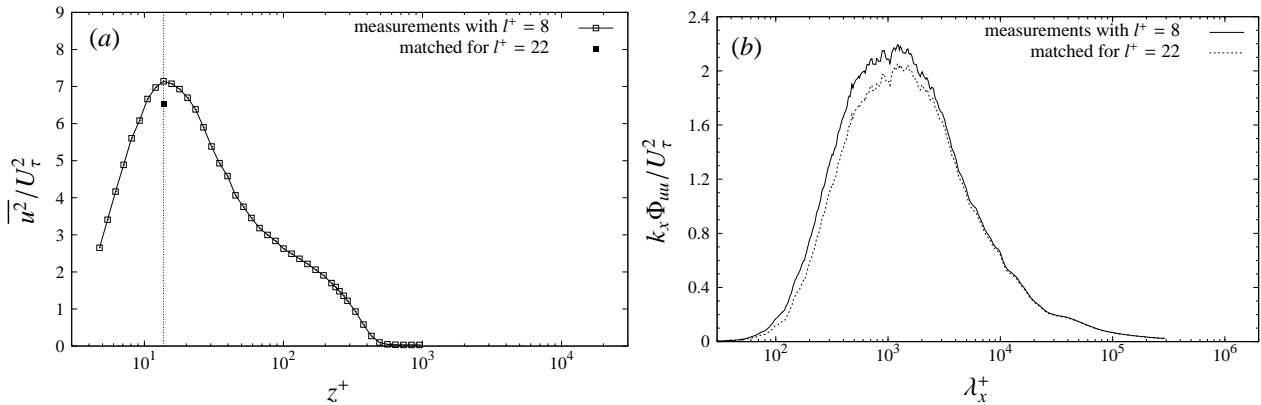


Figure 3: (a) Streamwise turbulence intensity results from Nottingham wind tunnel for  $Re_\tau = 500$ . (b) Corresponding premultiplied spectra versus wavelength at  $z^+ = 15$  compared to result where velocity signature has been modified to mimic a hot-wire with sensing length  $l^+ = 22$ .

peak intensity. This estimation is based on a correction scheme developed recently by Chin *et al.* [6] using a DNS dataset of wall turbulence to study the attenuation effects of a modeled hot-wire with finite spatial resolution. The difference between  $l^+ = 8$  and  $l^+ = 22$  is seen to be small. Figure 3(b) shows how the correction scheme effects the premultiplied  $u$ -spectra for  $z^+ = 15$ , where the area under the curves equals  $\overline{u^2}/U_\tau^2$ . The differences are again seen to be small and are confined to small wavelengths approximately  $\lambda_x^+ < 3000$ .

### 3. Turbulence intensities and spectra

Recently, substantial efforts have been devoted towards understanding the high Reynolds number scaling behaviour of the streamwise turbulence intensities ( $\overline{u^2}$ ) and the corresponding  $u$ -spectra, as well as to a lesser extent the other components of turbulence intensity ( $\overline{v^2}$ ,  $\overline{w^2}$ ) and Reynolds shear stress ( $-\overline{uw}$ ). Wall scaling has been widely used in computation schemes and assumes, like the mean flow, that the turbulence second order moments and spectra scale only with wall units in the near-wall region (for say,  $z/\delta < 0.15$ ). Alternative theories such as the attached eddy hypothesis [51, 45, 31] suggest otherwise and predict that while the wall-normal turbulence intensity and Reynolds shear stress ( $\overline{w^2}$  and  $-\overline{uw}$ ) will follow wall-scaling, the streamwise and spanwise components ( $\overline{u^2}$  and  $\overline{v^2}$ ) will not, and will depend on  $Re_\tau$ . Jimenez & Moser [21] and Jimenez &

Hoyas [20] considered these issues using DNS and experimental data and concluded that  $\overline{u^2}$  and  $\overline{v^2}$  do not follow wall-scaling, and nor does wall pressure or the local static pressure.

Many other recent studies have confirmed that  $\overline{u^2}^+$  is indeed dependent on Reynolds number (albeit weakly) [7, 34, 29]. Figure 4 shows results over the range of Reynolds numbers considered in the Melbourne and Nottingham wind tunnels. The data, which show a rise in the peak in  $\overline{u^2}^+$  with increasing Reynolds number, clearly suggest a failure of wall-scaling in the near-wall region.

In order to understand why the peak in  $\overline{u^2}^+$  changes with Reynolds number, it is helpful to consider the corresponding spectra, and this is shown in a premultiplied form in figure 5. It is worth noting that the representation here in terms of streamwise length-scale ( $\lambda_x^+$ ) is only a reflected mirror image of the conventional  $k_x \phi_{uu}/U_\tau^2$  versus  $\log(k_x^+)$  plot (equal areas under the curve will still denote equal energy). The figure shows that the near-wall  $u$ -spectra scale well in wall variables for all  $\lambda$  except the large scales. In other words, the increase in  $\overline{u^2}^+$  is directly attributed to an increase in energy due to large-scale motions, which do not scale on viscous wall variables. A similar trend has been observed on the spanwise pre-multiplied energy spectra of the streamwise velocity  $k_z \Phi_{uu}$  (see DNS studies Refs. [8, 1, 19, 13]), showing that near the wall there is an increase with  $Re_\tau$  of the energy of  $k_z \Phi_{uu}$  in the large spanwise

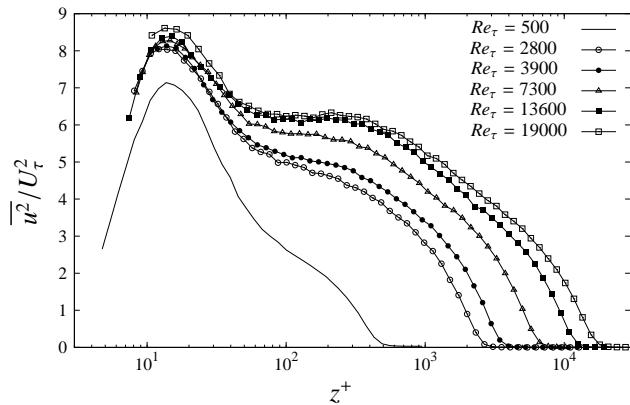


Figure 4: Reynolds number dependency of the streamwise turbulence intensity profile  $\overline{u^2}/U_\tau^2$ .

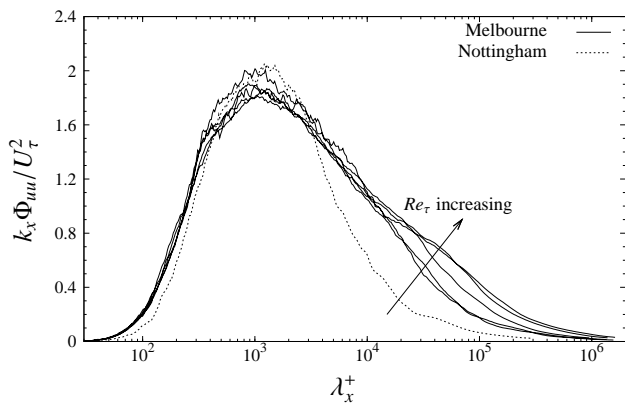


Figure 5: Pre-multiplied energy spectra of streamwise velocity fluctuations at the inner-peak location ( $z^+ = 15$ ).

wavelength  $k_z$ .

To see how large and small scale motions contribute to the broadband turbulence intensity, and to investigate this further we decompose the fluctuating velocity signals into a small-scale (where  $\lambda_x < \delta$ ) and a large-scale (where  $\lambda_x > \delta$ ) contribution using a simple cut-off spectral filter. The value  $\lambda_x = \delta$  is chosen after Hutchins & Marusic [15], and appears as a reasonable value provided the Reynolds number is sufficiently high to have a separation of inner and outer length scales. Figure 6(a) shows a streamwise broadband intensity profile decomposed in this way, and figure 6(b) shows how the decomposed components change with increasing Reynolds number. The small-scale component is seen to be invariant with Reynolds number across most of the boundary layer, while the outer-component clearly increases in magnitude across all wall-normal positions with increasing Reynolds number. The increasing influence in the near-wall region is noted, consistent with the spectral result in figure 5. The result in figure 6 shows that the  $\overline{u^2}/U_\tau^2$  profile can be considered to be the sum of two competing modes: a small viscous-scaled component primarily located in the near-wall region, and a larger outer-scaled component peaking in the

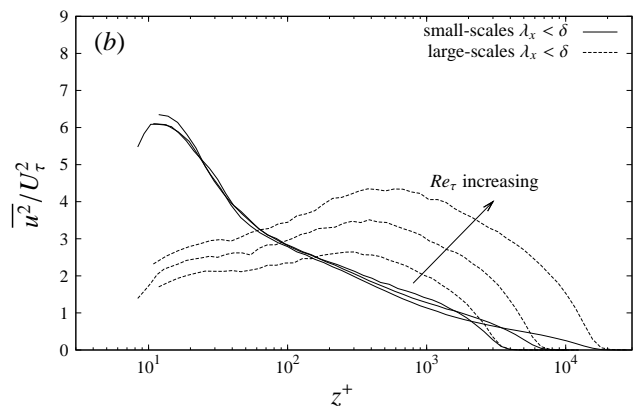
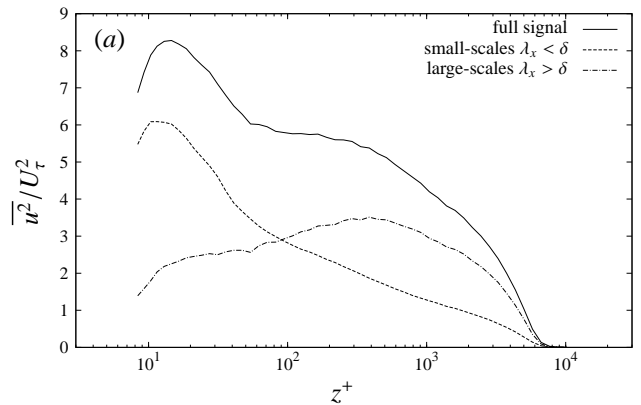


Figure 6: Scale decomposition of the streamwise turbulence intensity profile  $\overline{u^2}/U_\tau^2$ . (a) For  $Re_\tau = 7300$ , together with total (summed) contribution. (b)  $Re_\tau = 3900, 7300, 19000$ .

log region. There is considerable overlap between these modes, with the large-scale extending down to the wall, and a diminishing small-scale influence penetrating to the edge of the boundary layer.

To explore the role of the large-scale motions further, figure 7 gives an overview of the pre-multiplied streamwise energy spectra (shown with contours), across the full height of the turbulent boundary layer for a range of Reynolds numbers; with both inner (left column) and outer length scaling (right column). Two distinct peaks can be clearly observed in figure 7. The first peak, located in the near-wall region, is the energetic signature due to the viscous-scaled near-wall cycle of elongated high- and low-speed streaks (Kline *et al.* [25]), and is located at  $z^+ = 15$  and  $\lambda_x^+ = 1000$ . We will refer to this peak as the “inner-peak”, it corresponds to the location coincident with the peak value of  $\overline{u^2}^+$ . The large length-scale energy that encroaches at  $z^+ = 15$  with increasing Reynolds number, is seen to be part of a very large-scale structure associated with the second distinct peak in the spectrogram, which appears in the logarithmic region. We will refer to this peak as the “outer-peak”. It is of interest to note that this peak is not visible at low Reynolds numbers (where  $Re_\tau \lesssim 1700$ , see Ref. [16]) due to insufficient separation of scales and a diminishing strength at low  $Re$ . This outer peak is most likely the energetic signature due to

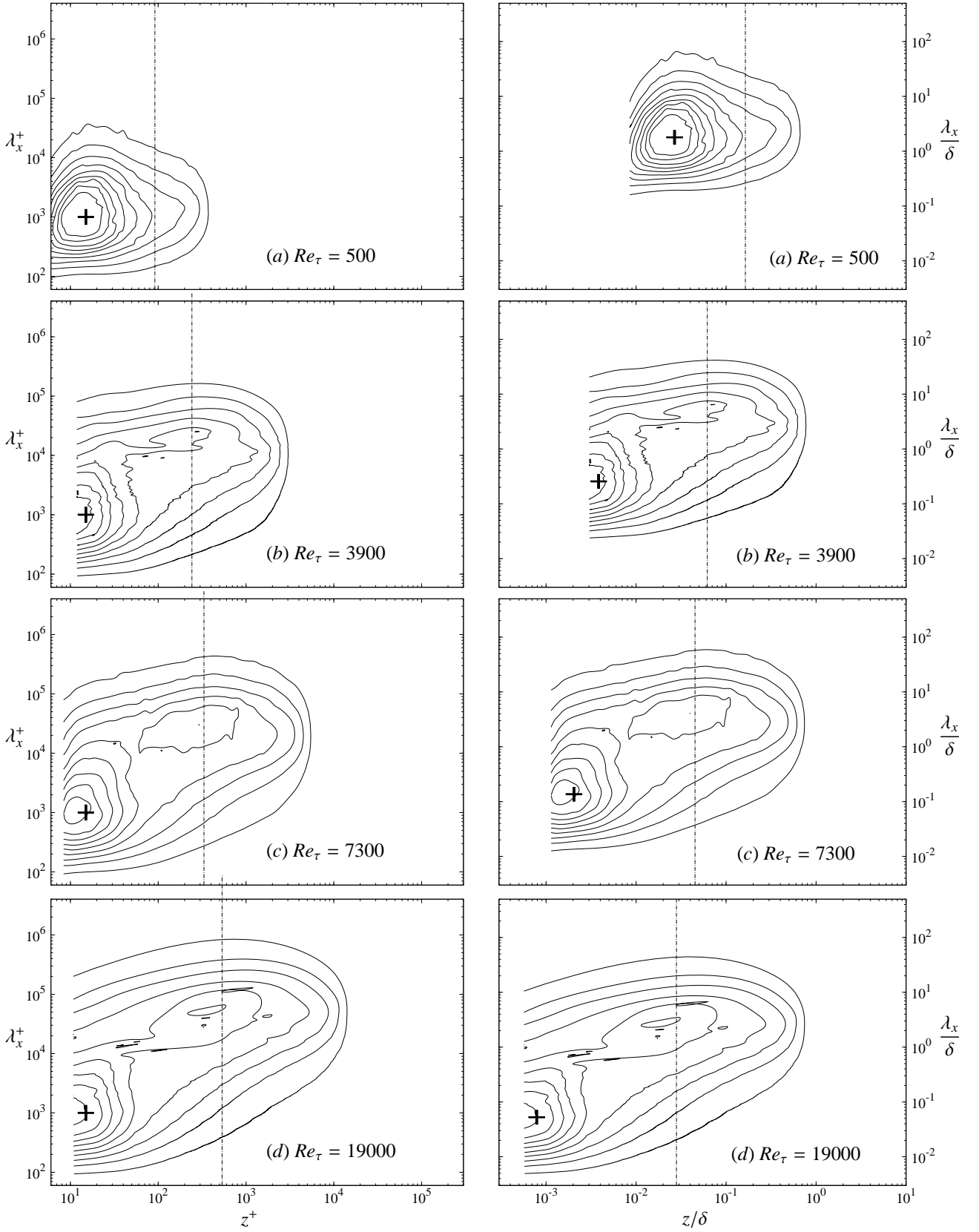


Figure 7: Reynolds number effect – Iso-contours of the pre-multiplied energy spectra of streamwise velocity fluctuation  $k_x \phi_{uuu} / U_\tau^2$ ; (a)  $Re_\tau = 500$ ; (b)  $Re_\tau = 3900$ ; (c)  $Re_\tau = 7300$ ; (d)  $Re_\tau = 19000$ ; Contour levels are from 0.2 to 1.8 in steps of 0.2; The large “+” marks the inner-peak location ( $z^+ = 15$ ,  $\lambda_x^+ = 1000$ ); The vertical dot-dashed line shows estimate of the middle of the log-layer ( $3.9Re_\tau^{1/2}$ ). The plots in the left column are scaled with inner variables, while the plots in the right-hand column are scaled with outer-scale variables.

the superstructure type events described by Hutchins & Marusic [15] (or VLSM as described by Kim & Adrian [23]). Hutchins & Marusic [15] showed that the magnitude of this outer peak (when  $k_x \phi_{uu}$  is scaled with  $U_\tau$ ) increases with Reynolds number. The wall-normal location of the outer peak is of particular interest. Initial observations of Hutchins & Marusic [15], suggest that the location of this peak scales in boundary layer thickness:  $z/\delta = 0.06$  and  $\lambda_x = 6\delta$ . However, here the data in figure 7, which cover a larger Reynolds number range, show the location of the outer peak to correspond well with the geometric center of the logarithmic region (on a log plot), which is indicated by the vertical dashed lines on each plot in figure 7. The location and scaling of the ‘outer peak’ in the  $u$ -spectra is of interest as it relates to the origin or source of the superstructures which, as discussed in the next section, exert a direct influence on the near-wall cycle in a mechanism akin to a pure amplitude modulation. Recently, Balakumar and Adrian [2] have studied the most energetic mode for  $k_x \Phi_{uu}$  in pipes, channels and zero-pressure gradient boundary layers, suggesting a possible scaling in outer units of the wavelength of the spectral peak of the VLSM.

The kinetic energy contribution coincident with the outer spectral peak is also of interest. If we assume that the location of the outer spectral peak follows  $z^+ = 3.9Re_\tau^{1/2}$  (consistent with the nominal centre of the log region) then the energy at this location is seen to increase, approximately following a logarithmic function of  $Re_\tau$ . This is shown in figure 8 (points with solid filled circles). Figure 8 also shows very high Reynolds number data from SLTEST experiments, which should be used with due caution due to measurement convergence and other uncertainties. However, these data together with the laboratory data indicate a consistent trend with the  $\overline{u^2}^+$  values at the inner spectral peak ( $z^+ \approx 15$ ) and the outer spectral peak ( $z^+ \approx 3.9Re_\tau^{1/2}$ ) both increasing nominally with the logarithm of  $Re_\tau$ . The slope for the logarithmic trend for  $z^+ \approx 15$  is debatable, and two lines are shown on the figure. One line (with slope 0.69) matches the slope of the line for the outer location, and in this event the  $\overline{u^2}^+$  value at  $z^+ \approx 15$  will continue to remain the dominant and sole peak across the layer as one extrapolates to very high Reynolds numbers. However, if one accepted the second line (with slope 0.39) then the trends shown in figure 8 indicate that a second peak in the  $\overline{u^2}^+$  profile will emerge at sufficiently high Reynolds number for a smooth wall flow (the level of  $\overline{u^2}^+$  in the log region will exceed the  $z^+ = 15$  value for  $Re_\tau \approx 10^6$ ). The critical level of  $Re_\tau$  at which such an outer peak in  $\overline{u^2}^+$  would appear is unclear, as the quantitative trends assigned here should be regarded as preliminary and are only an estimate based on the limited data that is available. Previous studies by Morrison *et al.* [38] in the Princeton superpipe have proposed that an outer peak does exist for  $\overline{u^2}^+$ . This has been the subject of some controversy, with concerns raised regarding the spatial resolution of these measurements. For example, Hutchins *et al.* [18] show that by increasing the sensing length of the hot-wire, the data shown in figure 4 will also appear with a second peak. Other experiments at very high Reynolds number at SLTEST by Metzger

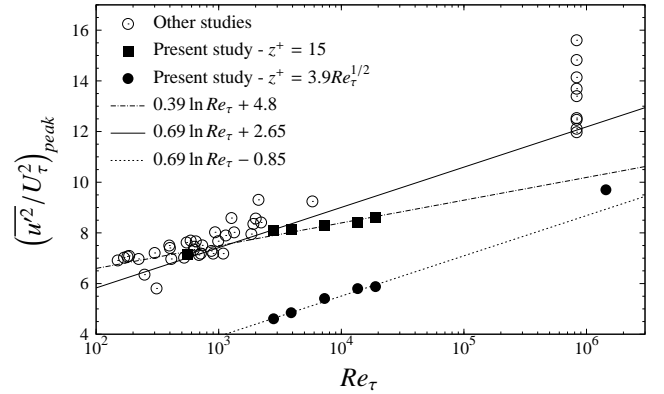


Figure 8: Variation of the peak value of the inner-scaled streamwise turbulence intensity with Reynolds number at the inner- (around  $z^+ = 15$ ) and outer-peak ( $z^+ \approx 3.9Re_\tau^{1/2}$ ) location. The data labeled ‘other studies’ is as reported in Fig. 8 in Ref. [15].

*et al.* [33] also show double peaks in the  $\overline{u^2}^+$  profile, but these have been attributed to roughness effects (which would reduce the level of the  $z^+ = 15$  peak). The trends in figure 8 suggest that the two peaks in the Metzger *et al.* [33] results might be present even if the flow was hydrodynamically smooth, but further data at high Reynolds number and with minimal spatial resolution effects are needed to resolve this.

### 3.1. Spanwise and wall-normal components

As mentioned above, there are considerably less studies that address the spanwise and wall-normal turbulence intensities and their spectra. Jimenez & Hoyas [20] review most of the existing experimental studies and show detailed comparisons of all components of spectra and cospectra for DNS of channel flows studies up to  $Re_\tau = 2000$ . They find that the large outer motions (or modes) of the spanwise and wall-normal velocities in boundary layers are stronger than found in channel flows, but conclude that similar outer-layer structures seem to exist in both channels and pipes and as in boundary layers at high Reynolds numbers.

Of the previous studies, most support wall scaling for the Reynolds shear stress and  $\overline{w^2}$  [26, 21], but the data is somewhat limited. Kunkel & Marusic [26] showed collapse of the  $w$ -spectra with inner (wall) scaling over three order of magnitude change in  $Re_\tau$  by making measurements in the log region of laboratory wind-tunnels and in the atmospheric surface layer. However, Zhao *et al.* [53] recently made similar two component hot-wire measurements in the Princeton Superpipe and suggest that  $\overline{w^2}^+$  and the  $w$ -spectra in the log region depend weakly on Reynolds number. Further experimental study seems warranted to resolve this issue and other ambiguities.

One of the difficulties here is that extremely small probe sizes are required to measure spanwise and wall-normal statistics in the near-wall region at high Reynolds numbers. This is highlighted in figure 9, which shows spectrograms for  $u$ ,  $v$  and  $w$  at  $Re_\tau = 7300$ , for  $\times$ -wire measurements taken in the Melbourne tunnel [17]. The absence of data in the near-wall region for  $v$

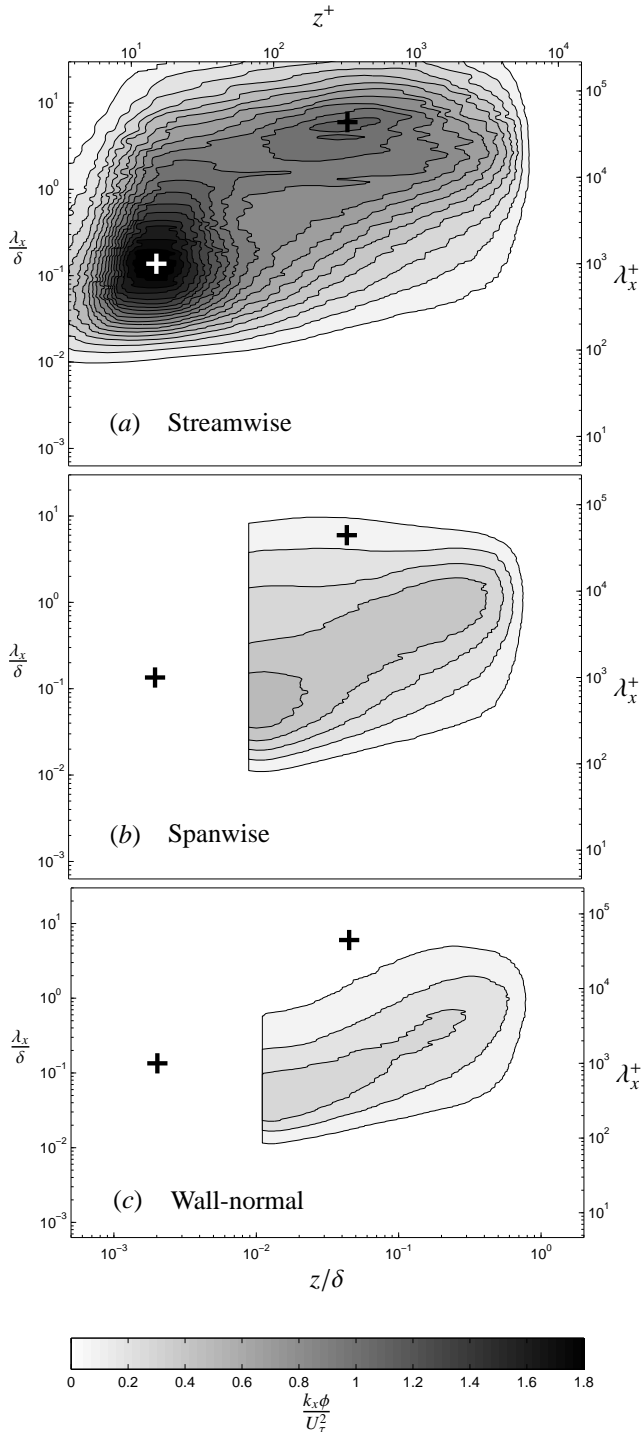


Figure 9: Contours of pre-multiplied energy spectra for (a) streamwise  $k_x \phi_{uu} / U_\tau^2$  (b) spanwise  $k_x \phi_{vv} / U_\tau^2$  (c) wall-normal  $k_x \phi_{ww} / U_\tau^2$  fluctuations. Contours are from 0.1 to 1.8 in steps of 0.1 (see gray scale). (+) symbols denote approximate locations of inner ( $z^+ \approx 15, \lambda_x^+ \approx 1000$ ) and outer ( $z^+ \approx 3.9Re_\tau^{1/2}, \lambda_x / \delta \approx 6$ ) peaks in  $u$  spectra. From Ref. [17]

and  $w$  (due to the size of the  $\times$ -wire probes) is very evident. For reference the location of the inner and outer peaks as identified in the  $u$ -spectra are also marked with (+) symbols on the spanwise ( $v$ ) and wall-normal ( $w$ ) spectra. Despite the lack of near-wall data, the spectra show some interesting trends. Im-

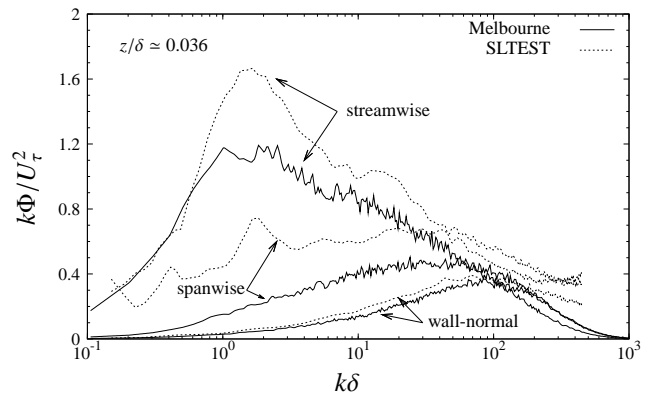


Figure 10: Comparison of the pre-multiplied energy spectra of the three velocity components at  $z/\delta = 0.036$  between laboratory boundary layer (Melbourne) and atmospheric surface layer (SLTEST).

mediately evident is the inclined ridge of energy for all components, where the length scale ( $\lambda$ ) is proportional to distance from the wall ( $z$ ). This is indicative of attached eddies. However, an important distinction between the  $v$  and  $w$  components for the near-wall region is that the wall-normal fluctuations lack a large-scale energetic contribution, in contrast to the spanwise fluctuations which exhibit near-wall energy at large ‘superstructure’ type length scales ( $\lambda_x \approx 6\delta$ ). Such behaviour is consistent with the notion of attached eddies, where the wall-normal fluctuations lack a large-scale component at the wall due to the ‘blocking-effect’, or equivalently, the image attached vortices in the wall [43]. It is also consistent with the notion that the superstructure events are associated with a very large-scale counter-rotating roll-mode [16], which produces a significant elongated spanwise signature (but not  $w$ ) for the region below the log region.

However, as indicated above, new high-quality experiments are needed over extended Reynolds number ranges to really address these issues. Questions certainly remain regarding the strength of this ‘roll-mode’ (and the corresponding  $v$  signature) and how this might change with Reynolds number. A number of studies at very high Reynolds number in the atmospheric surface layer (ASL) suggest that the spanwise intensity and spectra are significantly effected by increasing Reynolds number. An example of this is shown in figure 10 where the three components of velocity spectra are compared at a fixed location in the log region but where the Reynolds numbers are different by almost three orders of magnitude. The laboratory acquired data in figure 10 are taken in the Melbourne tunnel using hot-wires while the ASL data were measured using sonic anemometers at the SLTEST site in 2005 [15]. The ASL spectra are calculated from just one hour of data (taken from a period of prolonged neutral buoyancy and steady wind conditions), and thus the statistics for the largest scales cannot be considered fully-converged. Cautiously noting this caveat, the results in figure 10 do, however, strongly suggest that while the wall-normal component is little affected by the large change in Reynolds number, the spanwise and streamwise components will undergo

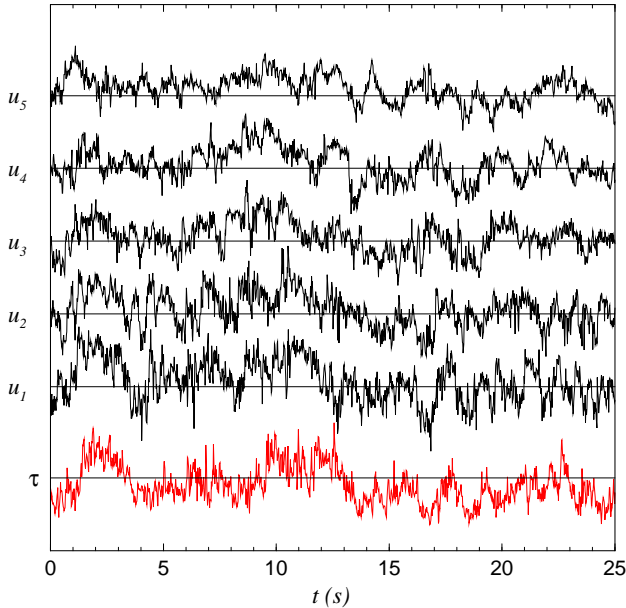


Figure 11: Time traces from Ref. [27] measured in the atmospheric surface layer,  $Re_\tau = O(10^6)$ . Fluctuating velocity at five wall-normal positions in the log layer are simultaneously shown with the fluctuating wall-shear stress ( $z/\delta = 0.0024, 0.005, 0.0091, 0.0165, 0.0293$ ). Significant coherence is noted between the wall shear stress and the velocity signals at this high Reynolds number.

dramatic changes, particularly with a large increase in spanwise kinetic energy associated with large length-scales. This is consistent with a strengthening of the superstructure events as described above.

#### 4. Large outer-scale interaction in near-wall region

Strengthening of the large-scale log-based superstructures implies that the near-wall region will be increasingly influenced at high Reynolds number and this extends to the skin-friction signature at the wall. Marusic & Heuer [27] conducted experiments at SLTEST and used a wall-normal array of sonic anemometers together with purpose-built skin-friction sensor that could measure time-resolved wall-shear stress [12]. A sample time trace from simultaneous measurements in this experiment are shown in figure 11. A high level of correlation is noted between the low-frequency components of the skin-friction signal and fluctuating streamwise velocity in the log region. This reaffirms the notion that the large-scale structures impose a “footprint” on the near-wall region. This conclusion itself is not new and has been previously observed in DNS studies in Refs. [1], [50] and [13], and more recently in Ref. [48], where the influence is noted of large scale motions at the wall. However, what is new in these ASL results, is the increasing magnitude of this influence at high Reynolds numbers.

An important feature of the “footprint” of the superstructures on the near-wall flow was noted by Hutchins & Marusic [15], who observed that the interaction of the large-scale motions was more than a mere superposition (or mean shift) on to the near-wall fluctuations (as per the attached eddy hypothesis [51]) but

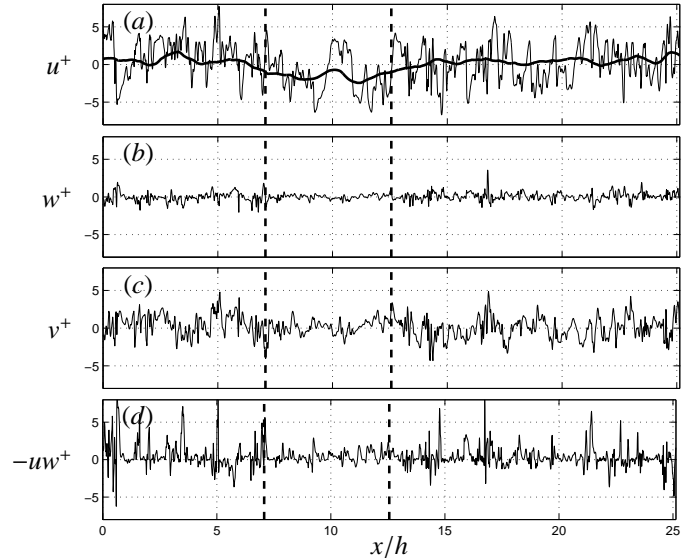


Figure 13: Example fluctuating velocity signals from the  $Re_\tau \approx 950$  channel of del Alamo *et al.* (2004) at  $z^+ = 15$ . (a) fluctuating  $u$  component, thicker line shows large-scale component; (b) wall-normal  $w$  fluctuation; (c) spanwise  $v$  fluctuation; (d) Reynolds shear stress fluctuation. Dashed vertical lines show region of negative large-scale fluctuation. Figure as shown in Ref. [16].

that rather the small-scale structures were subject to a high degree of amplitude modulation by the much larger scales that inhabit the log-region. An example of this is seen in figure 12 where a decomposition of a typical fluctuating signal  $u^+$  at wall-normal position  $z^+ = 15$  (inner-peak) is shown. Here a decomposition is used for scales below and above a cutoff length-scale, taken here to be  $\lambda_x/\delta = 1$  based on the spectra shown in figure 7. (Tests with different cutoff length-scales show that the basic trends are insensitive to choice of cutoff  $\lambda_x/\delta$ .) The large-scale component shown in figure 12(b) is highly correlated with the large-scale component in the log region, and is therefore taken as representative of the footprint of the superstructure at  $z^+ = 15$ . For the large-scale component shown in figure 12b, a prolonged region of negative fluctuation occurs (between the dashed lines), typical of the footprint caused by the decelerated portion of a superstructure-type event [15]. It appears that when this negative large-scale excursion occurs, the amplitude of the small-scale fluctuations  $u_s^+$  is significantly reduced (figure 12c). When similar analysis is conducted for a positive large-scale excursion, the opposite scenario is true and the amplitude of the small-scale fluctuations is increased. These results suggest that the low-wavenumber motions associated with the footprints of superstructure type events influence the near-wall  $u$  fluctuations in a manner akin to a pure amplitude modulation.

The modulating influence is not restricted to only the streamwise fluctuating velocity. For this we consider the DNS data at  $Re_\tau = 934$  of del Alamo *et al.* [9]. Here, the same trends are evident in the  $v$  and  $w$  fluctuations, both of which are more active under positive large-scale excitation (these trends are clear even though at these Reynolds numbers the footprint of the superstructure is relatively weak). This is seen in figure 13 which shows simultaneous signals for all three velocity com-

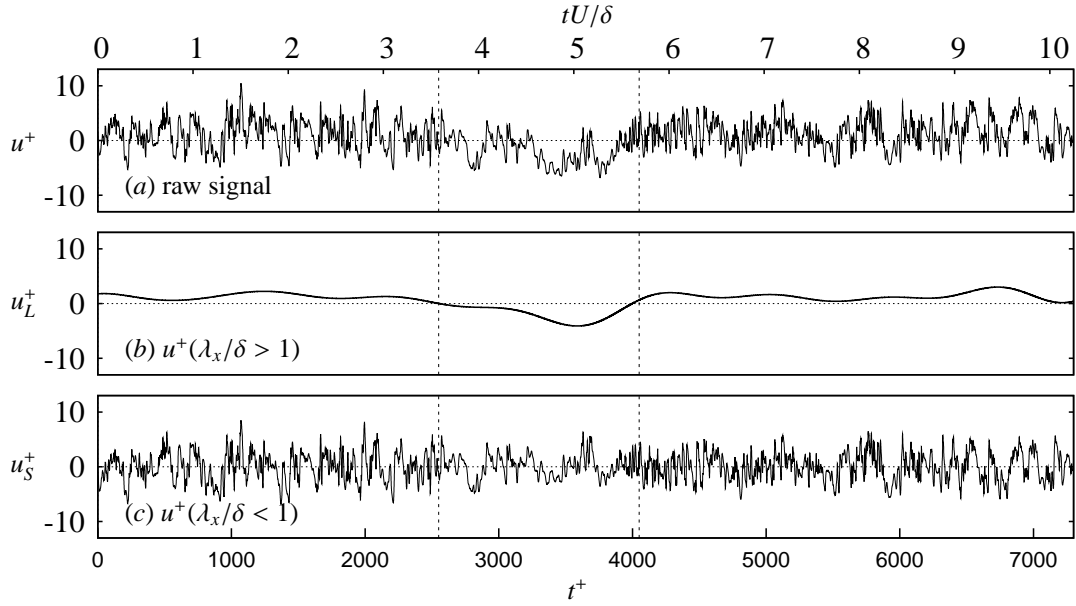


Figure 12: Example of fluctuating  $u$  signal in the near-wall region from Melbourne wind tunnel for  $Re_\tau = 7300$  at  $z^+ = 15$ ; (a) raw fluctuating component; (b) large-scale fluctuation  $\lambda_x/\delta > 1$ ; (c) small-scale fluctuation  $\lambda_x/\delta < 1$ ; Dashed vertical lines show region of negative large-scale fluctuation. Taken from Ref. [32].

ponents along with the instantaneous Reynolds shear stress  $uw$  at  $z^+ = 15$ . The small-scale activities for all signals are notably less intense during a large-scale negative  $u$  fluctuation (between the vertical dashed lines). As an additional point, it is evident from figure 13 that the wall-normal velocity fluctuation (figure 13b) does not have a large-scale component, while the  $u$  and  $v$  components (figure 13a,c) do, as noted in energy spectra by Hoyas & Jimenez [13] and previously in this paper in figure 9. Therefore, in the near-wall region, we have observed that under large-scale high-speed events (footprint of the superstructure), the local instantaneous Reynolds stresses (all components:  $\overline{u^2}$ ,  $\overline{v^2}$ ,  $\overline{w^2}$  and  $\overline{uw}$ ) are amplified, while the opposite is true under large-scale low-speed events. This is as expected since the local shear rate near the wall (and hence input of vorticity from the wall) is higher under high-speed events as compared with low-speed superstructure signatures. These findings are consistent with previous studies [3, 47] showing that large outer-scaled structures are active in rearranging and interacting with the near-wall structure. Furthermore, similar observations in the wall-shear stress fluctuations have been obtained in the DNS work of Abe *et al.* [1]. They shown that positive and negative regions of the streamwise wall-shear stress fluctuations correspond, respectively, to high- and low-speed events of the largest scales in the outer layer, whereas active regions in the spanwise wall-shear stress fluctuations coincide with high-speed regions of the very large-scale motions.

The modulation interaction is not easily detected in a Fourier representation. Because of the extremely low frequencies associated with the superstructures, the signature of the additional sideband frequencies generated by this amplitude modulation are difficult to determine in the power spectrum. The increasing importance of this nonlinear interaction across scales poses

several difficulties for the interpretation of the harmonic spectral decomposition of temporal signals. Mathis *et al.* [32] explore this further through analysis based on the Hilbert transform, which is well suited for quantifying modulation effects.

## 5. Towards a model for inner-outer interaction

The above results clearly show an influence of the large-scale superstructures in the near-wall region. Ideally we would like to build these observations into a mathematical model, which could enable a prediction to be made of the fluctuating velocity statistics in the near-wall region given only information about the large-scale signal in the log region.

As a first step towards this we can consider the viability of a model based on simple superposition. This will not capture the non-linear amplitude modulation effects, but such phase-related information is unlikely to effect the second-order statistics. Therefore, as a first attempt we propose a simple model for the prediction of a statistically representative signal at  $z^+ = 15$  as

$$u_{15}^+ = u_{15}^* + \alpha u_{LS}^+. \quad (2)$$

Here,  $u_{15}^+$  is the predicated  $u$ -signal at  $z^+ = 15$ ,  $u_{LS}$  is the fluctuating large-scale signal from the log-region,  $u_{15}^*$  is referred to as the statistically “universal” signal at  $z^+ = 15$  (normalized in wall units), and  $\alpha$  is a constant.  $u_{15}^*$  is the universal inner-scaled signal that would exist if there were no large-scale influence, and would be the total signal if wall-layer modeling applied. The large-scale signal,  $u_{LS}$ , is obtained from the  $u$ -signal in the log region (at a given  $z/\delta$  value, say 0.06) involving two steps. First, the  $u$ -signal is low-pass filtered to retain only large scales above, say,  $\lambda_x > \delta$ . Second, since we are equating a

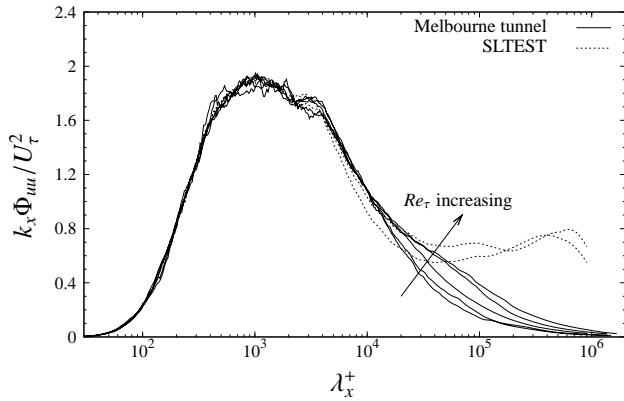


Figure 14: Prediction of pre-multiplied energy spectra at the inner-peak location ( $z^+ = 15$ )

log-region signal (from  $z/\delta = 0.06$ ) to  $z^+ = 15$  the measured  $u$ -signal is shifted forward in the streamwise direction (assuming Taylor's hypothesis with convection velocity equal to the local mean velocity) to account for the mean inclination angle of the large-scale structures ( $14^\circ$ ). This angle corresponds to the coherent structure angle of Marusic & Heuer [27], which they found to be invariant over three orders change in Reynolds number. The shift effectively corresponds to the time-delay that locates the maximum in a cross-correlation between the large scale  $u$ -signals at  $z/\delta = 0.06$  and  $z^+ = 15$ , and  $\alpha$  corresponds to the cross-correlation coefficient between these signals. These are assumed to be invariant and once obtained from a previous experiment, can be used at any Reynolds number.

The procedure for finding  $u_{15}^*$  is as follows. An experiment is conducted at an arbitrary Reynolds number (in this case  $Re_\tau = 7300$ ) in which the  $u$ -signals from two hot-wires mounted at  $z/\delta = 0.06$  and  $z^+ = 15$  are simultaneously sampled. From this  $\alpha$  (the correlation of the large-scale component between the two signals) is measured and found to be 0.70. Given  $\alpha$ , the universal signal  $u_{15}^*$  is then obtained by simply solving equation (2) as for this case  $u_{LS}$  and  $u_{15}^+$  are known.

With  $u_{15}^*$ , and  $\alpha$  known, and assumed to be invariant, predictions of  $u_{15}^+$  can now be made using equation (2) where the only input is the large-scale  $u$ -signal at  $z/\delta = 0.06$ . Figure 14 shows such (post-) predictions of spectra for the experiments previously carried out in the Melbourne tunnel and these compare extremely well with the true measurements shown in figure 5. Also, included in figure 14 are two predictions of what the spectra at  $z^+ = 15$  would be for  $Re_\tau = 6.5 \times 10^5$  and  $Re_\tau = 1.4 \times 10^6$ , which corresponds to experiments at SLTEST in Utah for which  $u_{LS}$  were available (in these cases from sonic anemometers). To test the validity of the model further, predictions were also made for  $\overline{u^2}^+$  and these results are shown in figure 15. The predictions are seen to agree very well, as expected since these are simply the area under the curves in figure 14.

The model given by equation (2) will likely need to be refined and extended to include the amplitude modulation effect described in the previous section. However, this would only be

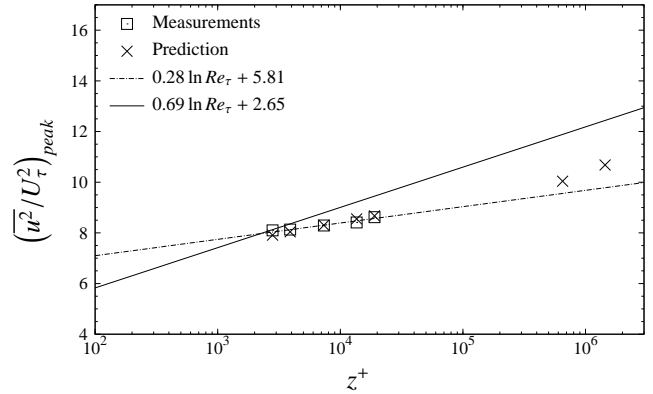


Figure 15: Prediction of streamwise turbulence intensity at the inner-peak location ( $z^+ = 15$ ) using equation (2).

needed if one required higher-order statistics and other quantities that involve phase information. For second-order statistics, equation (2) is seen to be largely adequate.

## 6. Conclusions and summary

An overview of Reynolds number effects in wall-bounded turbulence is offered. It is shown that the contribution from the logarithmic region to the overall turbulence production increases with Reynolds number. This would seem to imply that, as Reynolds number increases, the large-scale motions that inhabit this region, become increasingly important in terms of sustaining and producing turbulence (as compared to the near-wall cycle). This observation is consistent with the emergence (and subsequent strengthening) of a large-scale secondary energetic peak that has been noted in the spectra of the streamwise velocity fluctuations in the log region of high Reynolds number boundary layers. This secondary emergent peak is the energetic signature due to highly elongated (and correlated) meandering regions of spanwise alternating positive and negative  $u$  fluctuations that have been observed in the log and wake regions of wall-bounded turbulent flows (so-called superstructures or VLSM [23, 10, 15, 37, 36]). It is noted that the energetic signature due to these features increases with Reynolds number (as compared to the energy due to the near-wall cycle). It has been observed that these large-scale features maintain a 'footprint' or presence in the near-wall region. Through this mechanism, large-scale (log region) energy (which will get longer and stronger with  $Re$  as compared to the near-wall cycle) percolates down to the buffer and viscous sub-layers. Hence, the emergent view from careful comparisons of experimental data over extended Reynolds number ranges, is that the viscous-scaled near-wall peak of streamwise velocity fluctuations increases with Reynolds number (as opposed to the previously assumed viscous-scaling of near-wall fluctuations). In addition, it has been shown that the spanwise velocity component close to the wall also has a very large-scale energetic component. Data from the atmospheric surface layer has been presented which ten-

tatively suggest that this large-scale spanwise component will also grow in magnitude as Reynolds number increases.

In addition to the superimposition of large-scale log region energy onto the near-wall region, evidence is also presented which suggests a more subtle underlying non-linear mechanism whereby the large-scale structures amplitude modulate the small-scale fluctuating energy at the wall. This amplitude modulation occurs for all three velocity components and also the Reynolds shear stress. Thus the large-scale log-region motions appear to actively modulate or influence the production of turbulence at the wall. The superposition effect of the large-scale superstructures onto the near-wall region is seen to be well modeled with a simple mathematical model. It is able to predict the second-order statistical quantities of the velocity signal at  $z^+ = 15$  given a large-scale filtered signal from the logarithmic region. Though at this stage this model is preliminary, future extensions could be of great benefit to turbulence modeling efforts, where the near-wall signal is predicted given only large-scale information from the log region. Such information is precisely what is needed for an effective near-wall model for large-eddy simulations (LES) of high Reynolds number wall-bounded flows.

## Acknowledgements

The authors gratefully acknowledge the financial support of the Australian Research Council (DP0663499, FF0668703, DP0984577), and the Asian Office of Aerospace Research and Development (AOARD-094023)<sup>2</sup>.

## References

[1] Abe, H., Kawamura, H., Choi, H., 2004. Very large-scale structures and their effects on the wall shear-stress fluctuations in a turbulent channel flow up to  $Re_\tau = 640$ . *J. Fluids Eng.* 126, 835–843.

[2] Balakumar, B. J., Adrian, R. J., 2007. Large- and very-large scale motions in channel and boundary-layer flows. *Phil. Trans. R. Soc. Lond. A* 365, 665–681.

[3] Bandyopadhyay, P. R., Hussain, A. K. M. F., 1984. The coupling between scales in shear flows. *Phys. Fluids* 27 (9), 2221–2228.

[4] Barenblatt, G. I., Chorin, A. J., Hald, O. H., Prostokishin, V. M., 1997. Structure of the zero-pressure-gradient turbulent boundary layer. *Proc. Natl. Acad. Sci., USA* 29, 7817–7819.

[5] Carlier, J., Stanislas, M., 2005. Experimental study of eddy structures in a turbulent boundary layer using particle image velocimetry. *J. Fluid Mech.* 535, 143–188.

[6] Chin, C. C., Hutchins, N., Ooi, A. S. H., Marusic, I., 2009. Use of direct numerical simulation (DNS) data to investigate spatial resolution issues in measurements of wall-bounded turbulence. *Meas. Sci. Technol.* 20, 115401.

[7] DeGraaff, D. B., Eaton, J. K., 2000. Reynolds number scaling of the flat-plate turbulent boundary layer. *J. Fluid Mech.* 422, 319–346.

[8] del Álamo, J. C., Jiménez, J., 2003. Spectra of the very large anisotropic scales in turbulent channels. *Phys. Fluids* 15, 41–44.

[9] del Álamo, J. C., Jiménez, J., Zandonade, P., Moser, R. D., 2004. Scaling of the energy spectra of turbulent channels. *J. Fluid Mech.* 500, 135–144.

[10] Ganapathisubramani, B., Clemens, N. T., Dolling, D. S., 2006. Large-scale motions in a supersonic boundary layer. *J. Fluid Mech.* 556, 271–282.

[11] George, W. K., Castillo, L., 1997. Zero-pressure-gradient turbulent boundary layer. *Applied Mechanics Reviews* 50, 689–729.

[12] Heuer, W. D. C., Marusic, I., 2005. Turbulence wall-shear stress sensor for the atmospheric surface layer. *Meas. Sci. Technol.* 16, 1644–1649.

[13] Hoyas, S., Jiménez, J., 2006. Scaling of the velocity fluctuations in turbulent channels up to  $Re_\tau = 2003$ . *Phys. Fluids* 18, 011702.

[14] Hutchins, N., 2003. An investigation of large-scale coherent structures in fully developed turbulent boundary layers. Ph.D. thesis, University of Nottingham.

[15] Hutchins, N., Marusic, I., 2007. Evidence of very long meandering streamwise structures in the logarithmic region of turbulent boundary layers. *J. Fluid Mech.* 579 (1-28).

[16] Hutchins, N., Marusic, I., 2007. Large-scale influences in near-wall turbulence. *Phil. Trans. R. Soc. Lond. A* 365, 647–664.

[17] Hutchins, N., Marusic, I., Chong, M. S., 2007. Fully mapped energy spectra in a high Reynolds number turbulent boundary layer. In: *Proc 11th EUROMECH European Turbulence Conf.*

[18] Hutchins, N., Nickels, T. B., Marusic, I., Chong, M. S., 2009. Hot-wire spatial resolution issues in wall-bounded turbulence. *J. Fluid Mech.* 635, 103–136.

[19] Iwamoto, K., Kasagi, N., Suzuki, Y., 2004. Dynamical roles of large-scale structures in turbulent channel flow. In: *Computational Mechanics, WCCM VI in conjunction with APCOM'04.*

[20] Jimenez, J., Hoyas, S., 2008. Turbulent fluctuations above the buffer layer of wall-bounded flows. *J. Fluid Mech.* 611, 215–236.

[21] Jiménez, J., Moser, R. D., 2007. What are we learning from simulating wall turbulence? *Phil. Trans. R. Soc. Lond. A* 365, 715–732.

[22] Jimenez, J., Pinelli, A., 1999. The autonomous cycle of near-wall turbulence. *J. Fluid Mech.* 389, 335–359.

[23] Kim, K. C., Adrian, R., 1999. Very large-scale motion in the outer layer. *Phys. Fluids* 11, 417–422.

[24] Klewicki, J. C., Foss, J. F., Wallace, J. M., 1998. High Reynolds number [ $Re_\theta = O(10^6)$ ] boundary layer turbulence in the atmospheric surface layer above Western Utah's salt flats. In: *Donnelly, R. J., Sreenivasan, K. R. (Eds.), Flow at Ultra-High Reynolds and Rayleigh Numbers.* Springer.

[25] Kline, S. J., Reynolds, W. C., Schaub, F. A., Rundstadler, P. W., 1967. The structure of turbulent boundary layers. *J. Fluid Mech.* 30, 741–773.

[26] Kunkel, G. J., Marusic, I., 2006. Study of the near-wall-turbulent region of the high-Reynolds-number boundary layer using an atmospheric flow. *J. Fluid Mech.* 548, 375–402.

[27] Marusic, I., Heuer, W., 2007. Reynolds number invariance of the structure inclination angle in wall turbulence. *Phys. Rev. Lett.* 99, 114504.

[28] Marusic, I., Hutchins, N., 2008. Study of the log-layer structure in wall turbulence over a very large range of Reynolds number. *Flow Turbulence Combust.* 81, 115–130.

[29] Marusic, I., Kunkel, G. J., 2003. Streamwise turbulence intensity formulation for flat-plate boundary layers. *Phys. Fluids* 15, 2461–2464.

[30] Marusic, I., McKeon, B. J., Monkewitz, P., Nagib, H. M., Smits, A. J., Sreenivasan, K. R., 2009. Wall-bounded turbulent flows: recent advances and key issues. *J. Fluid Mech.* Under review.

[31] Marusic, I., Perry, A. E., 1995. A wall wake model for the turbulent structure of boundary layers. Part 2. Further experimental support. *J. Fluid Mech.* 298, 389–407.

[32] Mathis, R., Hutchins, N., Marusic, I., 2009. Large-scale amplitude modulation of the small-scale structures in turbulent boundary layers. *J. Fluid Mech.* 628, 311 – 337.

[33] Metzger, M., McKeon, B. J., Holmes, H., 2007. The near-neutral atmospheric surface layer: turbulence and non-stationarity. *Phil. Trans. R. Soc. Lond. A* 365 (1852), 859–876.

[34] Metzger, M. M., Klewicki, J. C., 2001. A comparative study of near-wall turbulence in high and low Reynolds number boundary layers. *Phys. Fluids* 13.

[35] Monkewitz, P., Chauhan, K., Nagib, H., 2007. Self-contained high-Reynolds-number asymptotics for zero-pressure-gradient turbulent boundary layers. *Phys. Fluids* 19, 115101.

[36] Monty, J. P., Hutchins, N., Ng, H., Marusic, I., Chong, M. S., 2009. A

<sup>2</sup>The views and conclusions contained herein are those of the authors and should not be interpreted as necessarily representing the official policies or endorsements, either expressed or implied, of the Air Force Research Laboratory or the U.S. Government.

- comparison of turbulent pipe, channel and boundary layer flows. *J. Fluid Mech.* 632, 431–442.
- [37] Monty, J. P., Stewart, J. A., Williams, R. C., Chong, M. S., 2007. Large-scale features in turbulent pipe and channel flows. *J. Fluid Mech.* 589, 147–156.
- [38] Morrison, J., McKeon, B., Jiang, W., Smits, A., 2004. Scaling of the streamwise velocity component in turbulent pipe flow. *J. Fluid Mech.* 508, 99–131.
- [39] Nagib, H., Chauhan, K., Monkewitz, P., 2007. Approach to an asymptotic state for zero pressure gradient turbulent boundary layers. *Phil. Trans. R. Soc. Lond. A* 365, 755.
- [40] Nickels, T. B., Marusic, I., Hafez, S. M., Chong, M. S., 2005. Evidence of the  $k^{-1}$  law in a high-Reynolds-number turbulent boundary layer. *Phys. Rev. Letters* 95, 074501.
- [41] Österlund, J. M., 1999. Experimental studies of zero pressure-gradient turbulent boundary-layer flow. Ph.D. thesis, Department of Mechanics, Royal Institute of Technology, Stockholm.
- [42] Panton, R. L., 2001. Overview of the self-sustaining mechanisms of wall turbulence. *Progress in Aerospace Sciences* 37, 341–383.
- [43] Perry, A. E., Chong, M. S., 1982. On the mechanism of wall turbulence. *J. Fluid Mech.* 119, 173–217.
- [44] Perry, A. E., Hafez, S., Chong, M. S., 2001. A possible reinterpretation of the Princeton superpipe data. *J. Fluid Mech.* 439, 395–401.
- [45] Perry, A. E., Henbest, S. M., Chong, M. S., 1986. A theoretical and experimental study of wall turbulence. *J. Fluid Mech.* 165, 163–199.
- [46] Perry, A. E., Marusic, I., Jones, M. B., 2002. On the streamwise evolution of turbulent boundary layers in arbitrary pressure gradients. *J. Fluid Mech.* 461, 61–91.
- [47] Rao, K. N., Narasimha, R., Badri Narayanan, M. A., 1971. The ‘bursting’ phenomena in a turbulent boundary layer. *J. Fluid Mech.* 48, 339–352.
- [48] Schlatter, P., Orlu, R., Li, Q., Brethouwer, G., Fransson, J. H. M., Johansson, A. V., Alfredsson, P. H., Henningson, D. S., 2009. Turbulent boundary layers up to  $Re = 2500$  studied through simulation and experiment. *Phys. Fluids* 21, 051702.
- [49] Schoppa, W., Hussain, F., 2002. Coherent structure generation in near-wall turbulence. *J. Fluid Mech.* 453, 57–108.
- [50] Toh, S., Itano, T., 2005. Interaction between a large-scale structure and near-wall structures in channel flow. *J. Fluid Mech.* 524, 249–262.
- [51] Townsend, A. A., 1976. *The Structure of Turbulent Shear Flow*. Vol.2, Cambridge University Press.
- [52] Zagarola, M. V., Smits, A. J., 1998. Mean-flow scaling of turbulent pipe flow. *J. Fluid Mech.* 373, 33–79.
- [53] Zhao, R., Smits, A., 2007. Scaling of the wall-normal turbulence component in high-Reynolds-number pipe flow. *J. Fluid Mech.* 576, 457–473.